JCTC Journal of Chemical Theory and Computation

Article

Cite This: J. Chem. Theory Comput. 2018, 14, 2127−2136

pubs.acs.org/JCTC

# Accuracy Assessment of *GW* Starting Points for Calculating Molecular Excitation Energies Using the Bethe−Salpeter Formalism

Xin Gui,[†] Christof Holzer,[†] and Wim Klopper*[,†,‡]

[†]Institute of Physical Chemistry, Theoretical Chemistry Group, Karlsruhe Institute of Technology (KIT), KIT Campus South, P.O. Box 6980, D-76049 Karlsruhe, Germany

[‡]Centre for Advanced Study (CAS) at The Norwegian Academy of Science and Letters, Drammensveien 78, N-0271 Oslo, Norway

Supporting Information

**ABSTRACT:** The performance of the Bethe−Salpeter equation (BSE) approach for the first-principles computation of singlet and triplet excitation energies of small organic, closed-shell molecules has been assessed with respect to the quasiparticle energies used on input, obtained at various levels of *GW* theory. In the corresponding *GW* computations, quasiparticle energies have been computed for *all* orbital levels by means of using full spectral functions. The assessment reveals that, for valence excited states, quasiparticle energies obtained at the levels of eigenvalue-only self-consistent (ev*GW*) or quasiparticle self-consistent theory (qs*GW*) are required to obtain results of comparable accuracy as in time-dependent density-functional theory (TDDFT) using a hybrid functional such as PBE0. In contrast to TDDFT, however, the BSE approach performs well not only for valence excited states but also for excited states with Rydberg or charge-transfer character. To demonstrate the applicability of the BSE approach, computation times are reported for a set of aromatic hydrocarbons. Furthermore, examples of computations of ordinary photoabsorption and electronic circular dichroism spectra are presented for $(C_{60})_2$ and $C_{84}$, respectively.

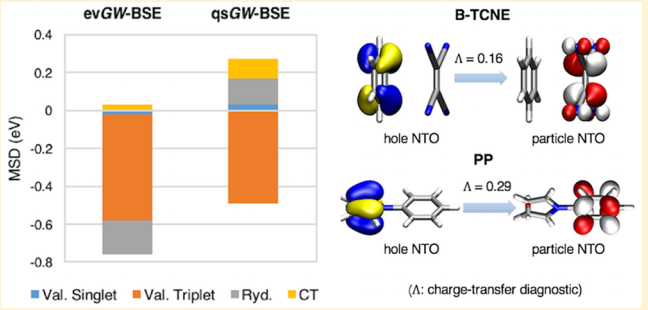




## 1. INTRODUCTION

The Bethe−Salpeter equation (BSE) approach—applied within the *GW* approximation—has in recent years attracted considerable interest in calculating molecular excitation energies.[1−26] Highly promising results have been reported in the cited works, and therefore, we recently decided to implement the BSE approach also in the TURBOMOLE program package.[27−29]

BSE computations normally require quasiparticle energies from preceding *GW* calculations on input, and the quality of computed excitation energies therefore depends much on the accuracy of the *GW* energy levels. There are various *GW* starting points for the BSE step, which are assessed in the present work. Often, the quasiparticle energies of the frontier orbitals (or a few orbitals about the Fermi level) are computed using efficient low-scaling methods such as stochastic techniques or by calculating the correlation self-energy first for imaginary frequencies employing a resolution-of-the-identity approximation and then for real frequencies by analytic continuation.[30−33] In contrast to this, in the present work, we compute the quasiparticle energies for *all* orbital levels by means of using the full spectral function in a molecular-orbital formalism. In particular, we shall investigate the linearized $G_0W_0$ method,[34] in which the quasiparticle energies are obtained from a first-order Taylor expansion about the Kohn−Sham (KS) or Hartree−Fock (HF) solution, as well as the $x_\alpha$-$G_0W_0$ scheme,[35] in which only an empirically scaled exchange self-energy is considered. The $G_0W_0$ approach is computationally efficient, but the lack of any self-consistency implies that the corresponding results depend on the KS or HF orbitals used in the calculation. On the other hand, fully self-consistent *GW* theory (sc*GW*) seems computationally too expensive.[36−38] Therefore, partially self-consistent schemes such as quasiparticle self-consistent *GW* theory (qs*GW*)[39,40] or eigenvalue-only self-consistent *GW* theory (ev*GW*)[30] can be good alternatives, although the latter scheme admittedly still depends on the KS or HF orbitals from a preceding calculation.

The present article is organized as follows: In Section 2, we briefly recapitulate the techniques implemented in the TURBOMOLE program package with respect to the computation of the Bethe−Salpeter excitation energies[27] (Subsection 2.1) and the *GW* quasiparticle energies (Subsection 2.2).[34,35,40] Computational details are given in Section 3. In Section 4, we assess the accuracy of the various *GW* starting points with respect to valence excited states (Subsection 4.1), Rydberg excited states (Subsection 4.2), and charge-transfer excited states (Subsection 4.3). In Section 5, we assess the performance of our program code by reporting timings measured for a few *GW* and BSE calculations (Subsection 5.1). We furthermore

**Received:** January 8, 2018
**Published:** March 2, 2018




DOI: 10.1021/acs.jctc.8b00014
J. Chem. Theory Comput. 2018, 14, 2127−2136

give examples of computed ordinary photoabsorption (Subsection 5.2) and electronic circular dichroism (Subsection 5.3) spectra computed at the *GW*-BSE level. Section 6 concludes the article.

## 2. IMPLEMENTATION

**2.1. BSE Approach.** The matrix elements of the BSE approach—in the static screened-exchange approximation—are given in ref 27, where also the efficient calculation of the screened potential using the resolution-of-the-identity (RI) approximation is described, as implemented in the TURBOMOLE program package.

We construct the BSE orbital-rotation matrices $\mathbf{A} + \mathbf{B}$ and $\mathbf{A} - \mathbf{B}$, which are defined as

$$(A + B)_{ia,jb} = (\varepsilon_a - \varepsilon_i)\delta_{ij}\delta_{ab} + 2v_{ia,jb} - W_{ij,ab} - W_{ib,aj} \tag{1}$$

and

$$(A - B)_{ia,jb} = (\varepsilon_a - \varepsilon_i)\delta_{ij}\delta_{ab} - W_{ij,ab} + W_{ib,aj} \tag{2}$$

where $v_{pq,rs} = (qp|rs)$ is a two-electron Coulomb integral, $W_{pq,rs}$ a two-electron static screened-exchange integral, and $\varepsilon_p$ a quasiparticle (QP) energy of a preceding *GW* calculation.[27] We use the indices $i, j$ to denote occupied spin orbitals and $a, b$ to denote virtual spin orbitals. It is assumed that the orbitals are real-valued functions. Note that $W_{pq,rs} = 0$ when the direct random-phase approximation (dRPA) is applied.

After constructing the $\mathbf{A} + \mathbf{B}$ and $\mathbf{A} - \mathbf{B}$ matrices, the eigenvectors needed for the response function are obtained by solving the symmetric eigenvalue problem (see ref 41)

$$\tilde{\mathbf{L}}^{\mathrm{T}}(\mathbf{A} + \mathbf{B})\tilde{\mathbf{L}}\tilde{\mathbf{Z}} = \tilde{\mathbf{Z}}\boldsymbol{\omega}^2 \tag{3}$$

where $\boldsymbol{\omega}$ is a diagonal matrix and

$$(\mathbf{A} - \mathbf{B}) = \tilde{\mathbf{L}}\tilde{\mathbf{L}}^{\mathrm{T}} \tag{4}$$

After solving the eigenvalue equation, the eigenvectors $\mathbf{Z}$ are obtained as

$$\mathbf{Z} = \tilde{\mathbf{L}}\tilde{\mathbf{Z}}\boldsymbol{\omega}^{-1/2} \tag{5}$$

$\tilde{\mathbf{L}}\tilde{\mathbf{L}}^{\mathrm{T}}$ is the Cholesky decomposition of the Hermitian, positive definite matrix $\mathbf{A} - \mathbf{B}$. Note that this decomposition can not only be used for "pure" density functionals (i.e., without exchange) but also when exchange contributions are incorporated—as long as $\mathbf{A} - \mathbf{B}$ is a Hermitian, positive definite matrix.

The evaluation of four-index, two-electron integrals $(pq|rs)$ is significantly accelerated by means of using the RI approximation,

$$(pq|rs) \approx \sum_{PQ} (pq|P)(\mathbf{V}^{-1})_{PQ}(Q|rs) \tag{6}$$

This is accomplished by means of a Cholesky decomposition of the symmetric, positive definite matrix $\mathbf{V}$ containing two-index, two-electron integrals $V_{PQ} = (P|Q)$ over (real-valued) functions of the auxiliary basis set,

$$\mathbf{V} = \mathbf{L}\mathbf{L}^{\mathrm{T}} \tag{7a}$$

$$R_{P,\mathrm{rs}} = \sum_{Q} (\mathbf{L}^{-1})_{PQ}(Q|rs) \tag{7b}$$

$$v_{pq,\mathrm{rs}} \equiv (qp|rs) \approx \sum_{Q} (\mathbf{R}^{\mathrm{T}})_{qp,Q} R_{Q,\mathrm{rs}} \tag{7c}$$

In eq 6, $(Q|rs)$ is a three-index, two-electron integral.

**2.2. *GW* Methods.** The first implementations of the various *GW* approximations in the TURBOMOLE program package are described in refs 34, 35, and 40. However, in these initial implementations, the orbital-rotation matrices were assembled using an atomic-orbital (AO) based formalism. In contrast to this, a symmetry-adapted molecular-orbital (MO) based formalism is adopted in the present work. In a spin−orbital formalism the matrix elements are calculated as follows: for the calculation of the quasiparticle energies in the $G_0W_0$, ev*GW*, and qs*GW* approximations, the required integrals $(ia|\rho_{jb})$ are evaluated by first contracting the excitation vectors contained in the matrix $\mathbf{Z}^{\mathrm{dRPA}}$ with the three-index intermediates $R_{Q,kc}$,

$$U_{Q,jb} = \sum_{kc} R_{Q,kc} Z^{\mathrm{dRPA}}_{kc,jb} \tag{8}$$

Note that the dRPA approximation is applied when computing the excitation vectors $\mathbf{Z}^{\mathrm{dRPA}}$, using quasiparticle energies $\varepsilon_p$ in the cases of the ev*GW* and qs*GW* methods, but KS or HF orbital energies $\varepsilon_p$ in the case of the $G_0W_0$ method. Hence, the orbital−rotation matrices in the direct random-phase approximation take the form

$$(A + B)^{\mathrm{dRPA}}_{ia,jb} = (\varepsilon_a - \varepsilon_i)\delta_{ij}\delta_{ab} + 2v_{ia,jb} \tag{9a}$$

$$(A - B)^{\mathrm{dRPA}}_{ia,jb} = (\varepsilon_a - \varepsilon_i)\delta_{ij}\delta_{ab} \tag{9b}$$

The final two-electron integrals are computed in the RI approximation as

$$(ia|\rho_{jb}) \approx \sum_{Q} (\mathbf{R}^{\mathrm{T}})_{ia,Q} U_{Q,jb} \tag{10}$$

and the matrix elements of the self-energy are obtained from these integrals as

$$\langle p|\Sigma_c(\varepsilon_s)|q\rangle = \sum_{k}\sum_{jb} (kp|\rho_{jb})(kq|\rho_{jb})D^{+}_{k,s,jb} + \sum_{c}\sum_{jb} (cp|\rho_{jb})(cq|\rho_{jb})D^{-}_{c,s,jb} \tag{11}$$

where

$$D^{\pm}_{r,s,jb} = \frac{\varepsilon_s - \varepsilon_r \pm \omega_{jb}}{(\varepsilon_s - \varepsilon_r \pm \omega_{jb})^2 + \eta^2} \tag{12}$$

For the $G_0W_0$ and ev*GW* approximations, only the diagonal matrix elements $\langle p|\Sigma_c(\varepsilon_p)|p\rangle$ are required, whereas for the qs*GW* approximation, also the off-diagonal matrix elements $\langle p|\Sigma_c(\varepsilon_s)|q\rangle$ are required, with $s = \{p, q\}$. In the qs*GW* model, the Fock matrix reads

$$F_{pq} = h_{pq} + J_{pq} - K_{pq} + \frac{1}{2}\langle p|\Sigma_c(\varepsilon_p) + \Sigma_c(\varepsilon_q)|q\rangle \tag{13}$$

where $\mathbf{h}$ is the one-electron Hamiltonian and $\mathbf{J}$ and $\mathbf{K}$ the usual Coulomb and exchange matrices, respectively, as they occur in Hartree−Fock theory.

## 3. COMPUTATIONAL DETAILS

All calculations in the present article were performed with the TURBOMOLE program package.[28,29] The underlying Hartree−Fock and density functional theory (DFT) computations were carried out with the modules DSCF and RIDFT. The subsequent approximate coupled-cluster singles−doubles calculations


DOI: 10.1021/acs.jctc.8b00014
J. Chem. Theory Comput. 2018, 14, 2127−2136

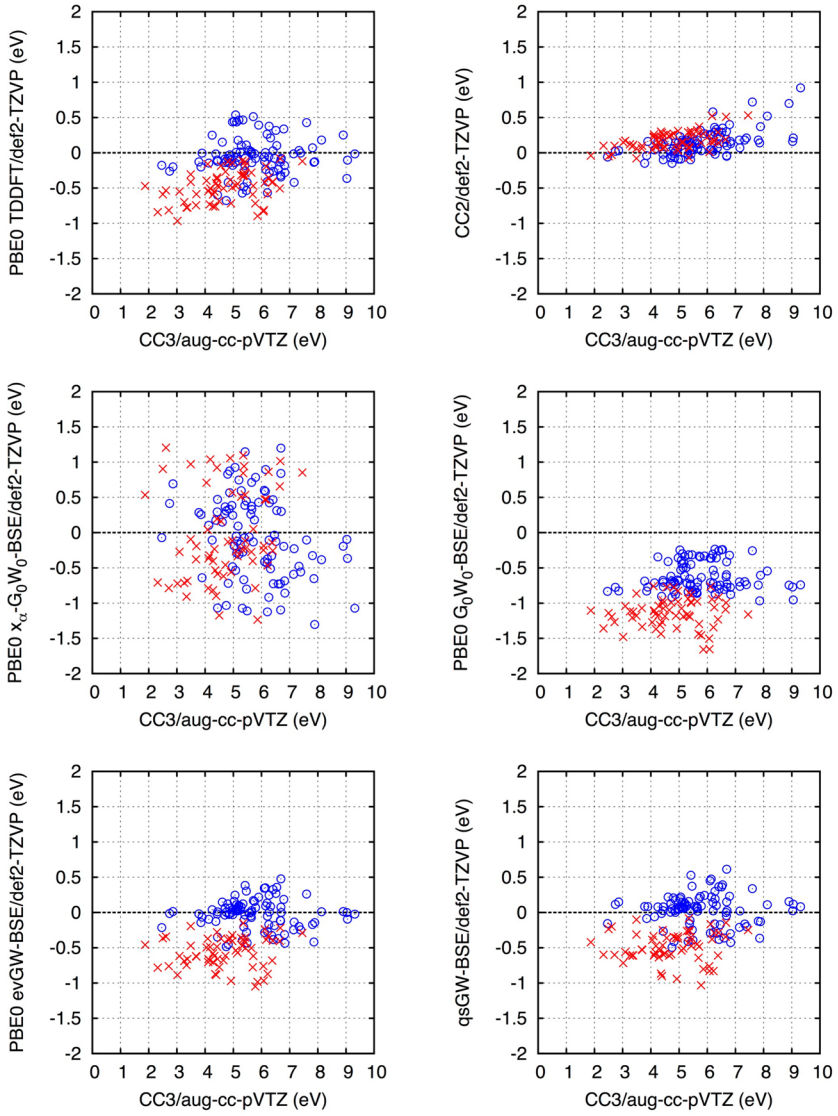


**Figure 1.** Computed singlet (blue circles) and triplet (red crosses) excitation energies. Plotted are the deviations from the reference CC3/aug-cc-pVTZ values.

(CC2) and approximate coupled-cluster singles–doubles–triples calculations (CC3, not yet part of the public release of the TURBOMOLE program package) computations were done with the modules RICC2 and CCSDF12, respectively. TDDFT and *GW*-BSE computations were carried out with the ESCF module. The resolution-of-the-identity (RI) approximation was used for all two-electron integrals, and the frozen-core approximation was applied in the coupled-cluster calculations.

In the Hartree–Fock and DFT computations, we used the self-consistent-field convergence criterion `scfconv = 8` and DFT grid size m4 (modified grid 4). In the coupled-cluster computations, default convergence thresholds were used. For the TDDFT and *GW*-BSE computations, the convergence criterion was set to `rpaconv = 6` (in the ev*GW* calculations, `rpaconv = 4` was used). Furthermore, the keywords `offpq = 0.03` and `eta = 0.001` were used in the qs*GW* calculations to achieve rapid convergence.

All orbital and auxiliary basis sets used in the present work were taken from the TURBOMOLE basis-set library.[29] Note that "MP2-fitting" auxiliary basis sets (denoted `cbas` in TURBOMOLE jargon) were used throughout the present work, except for the expansion of the total electron density in the ground-state DFT calculations, where the "Coulomb-fitting" auxiliary basis set was used (denoted `jbas` in TURBOMOLE jargon).

## 4. ACCURACY ASSESSMENT

**4.1. Valence Excited States.** The well-known benchmark set established by Thiel and co-workers[42−44] consists of 28 small- and medium-sized organic molecules. Theoretical best estimates (TBEs) were proposed for the vertical excitation energies of 104 singlet and 63 triplet valence excited states based on an extensive literature study as well as on ab initio computations performed by the authors. The calculations were initially done in 2008[42] using both CASPT2 (complete-active-space perturbation theory to second order) and a hierarchy of coupled-cluster methods with the TZVP basis set. The computed CASPT2/TZVP excitation energies were taken as reference values for the singlet excited states due to the existence of normally at least one state in each molecule with a CC3 single-excitation weight below 90%. Computed CC3/TZVP excitation energies were adopted as reference values for the triplet states because their CC3 single-excitation weights


DOI: 10.1021/acs.jctc.8b00014
J. Chem. Theory Comput. 2018, 14, 2127−2136

Table 1. Deviations of Singlet Excitation Energies (eV) Obtained in the def2-TZVP Basis with Respect to the CC3/aug-cc-pVTZ Reference[a]

| | TDDFT | CC2 | $x_\alpha$-$G_0W_0$-BSE[b] | $G_0W_0$-BSE | ev$GW$-BSE | qs$GW$-BSE |
|---|---|---|---|---|---|---|
| mean | −0.06 | 0.14 | −0.06 | −0.63 | −0.02 | 0.03 |
| mean abs. | 0.21 | 0.17 | 0.50 | 0.63 | 0.16 | 0.18 |
| RMS | 0.27 | 0.23 | 0.59 | 0.66 | 0.21 | 0.23 |
| std. dev. | 0.26 | 0.18 | 0.59 | 0.21 | 0.21 | 0.23 |
| max. abs. | 0.68 | 0.92 | 1.30 | 0.97 | 0.48 | 0.64 |
| median abs. | 0.15 | 0.14 | 0.41 | 0.70 | 0.12 | 0.14 |

[a]The PBE0 functional was used in the ev$GW$-BSE, $G_0W_0$-BSE, $x_\alpha$-$G_0W_0$-BSE, and TDDFT calculations. [b]$\alpha_{opt}$ = 0.65.

Table 2. Deviations of Triplet Excitation Energies (eV) Obtained in the def2-TZVP Basis with Respect to the CC3/aug-cc-pVTZ Reference[a]

| | TDDFT | CC2 | $x_\alpha$-$G_0W_0$-BSE[b] | $G_0W_0$-BSE | ev$GW$-BSE | qs$GW$-BSE |
|---|---|---|---|---|---|---|
| mean | −0.48 | 0.17 | −0.03 | −1.14 | −0.56 | −0.49 |
| mean abs. | 0.48 | 0.18 | 0.56 | 1.14 | 0.56 | 0.49 |
| RMS | 0.53 | 0.22 | 0.65 | 1.16 | 0.60 | 0.53 |
| std. dev. | 0.23 | 0.13 | 0.65 | 0.21 | 0.22 | 0.21 |
| max. abs. | 0.97 | 0.53 | 1.24 | 1.66 | 1.05 | 1.03 |
| median abs. | 0.47 | 0.15 | 0.53 | 1.12 | 0.54 | 0.48 |

[a]The PBE0 functional was used in the ev$GW$-BSE, $G_0W_0$-BSE, $x_\alpha$-$G_0W_0$-BSE, and TDDFT calculations. [b]$\alpha_{opt}$ = 0.76.

were typically above 95%. In most cases the CASPT2 and CC3 results were in close mutual agreement. Later in 2010,[44] however, the previous TZVP values were replaced by improved results obtained with the larger aug-cc-pVTZ basis set in an attempt to account for high-lying valence states with rather diffuse character. Because the CASPT2 procedure was less standardized with the more diffuse aug-cc-pVTZ basis, CC3 values were taken for both singlets and triplets except for five singlets with single-excitation weights below 80%, where CASPT2 values were used instead.

For the singlet excited states of the four nucleobases, the TBE values were taken from the literature at the CC2 level because all-electron CC3 calculations had thus far not been feasible for these molecules. However, the accuracy of the CC2 model is rather questionable in these systems as pointed out by Szalay and co-workers,[45] who extended the benchmark set with CC3/TZVP data (computed in the frozen-core approximation) for all of the molecules, especially for the nucleobases, and who revisited the particularly problematic cases of the four nucleobases in a subsequent paper.[46] It has been shown that, in comparison with CC3 data, the CC2 model tends to underestimate the excitation energies of $n \rightarrow \pi^*$ transitions (with a mean error of ca. −0.03 eV) while it tends to overestimate those of $\pi \rightarrow \pi^*$ transitions (with a mean error of ca. 0.09 eV). In order to make the benchmark more consistent and reliable, we decided to adopt the CC3/TZVP results with the ΔCC2/aug-cc-pVTZ basis-set correction,

$$\Delta\text{CC2/aug-cc-pVTZ} = \text{CC2/aug-cc-pVTZ} - \text{CC2/TZVP} \quad (14)$$

as reference values for the four nucleobases. Such an incremental scheme has been justified in ref 43, where the CC3/TZVP+ΔCC2/aug-cc-pVTZ estimates were found to be very close to the CC3/aug-cc-pVTZ results (normally, agreement within 0.1 eV was achieved).

Since the BSE model can only treat excited states dominated by single excitations, we excluded states with obvious double-excitation character. The criterion of CC3/TZVP single-excitation weight[42] below 80% (as in ref 44) was adopted. This applied to the $2^1A_g$ states of butadiene, hexatriene, and octatetraene, the $2^1A_1$ state of cyclopentadiene, the $2^1E_{2g}$ state of benzene, the $3^1A_g$ state of naphthalene, and the $1^1B_{3u}$ state of benzoquinone, as well as to the doubly excited $1^1B_{3g}$ state of tetrazine, where coupled-cluster methods fail. Note that the $1^1B_{1g}$ state of naphthalene also has a single-excitation weight slightly below 80%, but in this case the CC3/aug-cc-pVTZ and CASPT2/aug-cc-pVTZ results were rather close to each other (the difference was smaller than 0.05 eV). This mutual agreement is much better than for the states mentioned above, and thus we regard the $1^1B_{1g}$ state of naphthalene as a singly excited state. Moreover, special attention should also be paid to the singlet excited states of a few molecules, namely, the $^1A''$ states of imidazole, the $^1A_1$ states of formaldehyde and acetone, the $^1A'$ states of formamide, acetamide, and propanamide, and the $^1A''$ states of uracil, where low-lying Rydberg states were found to lie in between the valence states. Significant valence−Rydberg mixing was detected in some cases.[45] We have analyzed the corresponding natural transition orbitals (NTOs) for a quantitative description of the character of these states, and it was found that the $2^1A'$ state of the three amides suffers from strong valence−Rydberg mixing. A clear assignment was not possible for these states, which were excluded from our performance assessment. Therefore, 93 singlet excited states and 63 triplet excited states were left in the benchmark. Instead of using the TBE values published in the literature, we adopt the CC3/aug-cc-pVTZ data as reference values for all of the states (see the Supporting Information for details).

The deviations of the computed singlet and triplet excitation energies from the respective CC3/aug-cc-pVTZ reference values are plotted in Figure 1, and the statistical analyses of singlets and triplets are listed in Tables 1 and 2, respectively, together with graphical representations in Figures 2 and 3, respectively. As can be clearly seen, the CC2 model provides an accurate and balanced description for both singlet and triplet excited states. The $x_\alpha$-$G_0W_0$-BSE energies spread too far from the reference while the $G_0W_0$-BSE energies are too small on


DOI: 10.1021/acs.jctc.8b00014
J. Chem. Theory Comput. 2018, 14, 2127−2136

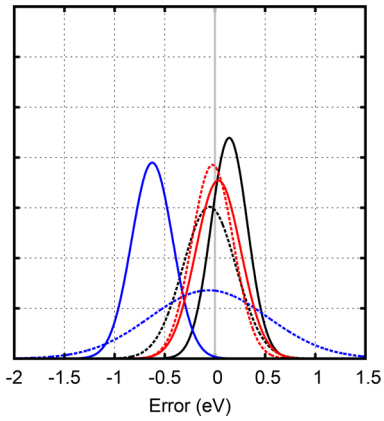


**Figure 2.** Representation of the statistical analysis of Table 1 as normalized Gaussian distributions. Shown are the error distributions for the TDDFT (dashed black line), CC2 (solid black), $x_\alpha$-$G_0W_0$-BSE (dashed blue), $G_0W_0$-BSE (solid blue), ev*GW*-BSE (dashed red), and qs*GW*-BSE (solid red) models.

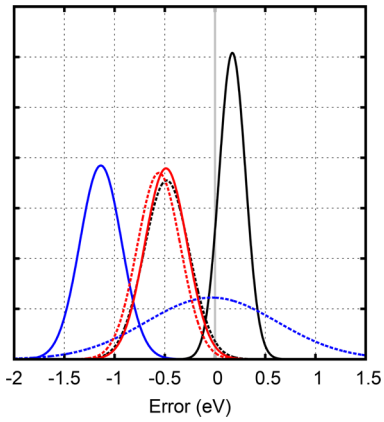


**Figure 3.** Representation of the statistical analysis of Table 2 as normalized Gaussian distributions. Shown are the error distributions for the TDDFT (dashed black line), CC2 (solid black), $x_\alpha$-$G_0W_0$-BSE (dashed blue), $G_0W_0$-BSE (solid blue), ev*GW*-BSE (dashed red), and qs*GW*-BSE (solid red) models.

average, and hence these two methods are not recommended in combination with the PBE0 functional. However, findings of other studies suggest that hybrid functionals that incorporate more HF exchange provide results closer to qs*GW*.[40] The TDDFT, ev*GW*-BSE, and qs*GW*-BSE methods show similar performance, and in the case of singlet states, they achieve an accuracy that is comparable to that of the CC2 model. However, the TDDFT, ev*GW*-BSE, and qs*GW*-BSE methods systematically underestimate the triplet excitation energies. We noticed that, when performing the calculations with HF orbitals, the ev*GW*-BSE method yielded surprisingly good triplet excitation energies, but then the singlet excited states were overestimated and became much less accurate than those obtained with PBE0 Kohn−Sham orbitals. This underestimation of the triplet energies by the ev*GW*-BSE model has also been addressed earlier in ref 7, where the authors suggested that a self-consistent *GW* approach might improve the results. However, as shown in the present work, although the dependence on the reference orbitals is removed by the qs*GW*-BSE model, it hardly yields any improvement in comparison to the ev*GW*-BSE model. The triplet excitation energies are still much too small in the qs*GW*-BSE model. The reason for this behavior is not clear yet, and further studies are needed.

We have performed additional aug-cc-pVTZ calculations using the CC2, TDDFT, ev*GW*-BSE, and qs*GW*-BSE methods to investigate their basis-set dependence. The statistical analyses with respect to the CC3/aug-cc-pVTZ reference data are given in Tables 3 and 4 while Tables 5 and 6 provide

**Table 3. Deviations of Singlet Excitation Energies (eV) Obtained in the aug-cc-pVTZ Basis with Respect to the CC3/aug-cc-pVTZ Reference[a]**

| | TDDFT | CC2 | ev*GW*-BSE | qs*GW*-BSE |
|---|---|---|---|---|
| mean | −0.13 | 0.03 | −0.24 | −0.04 |
| mean abs. | 0.23 | 0.09 | 0.26 | 0.17 |
| RMS | 0.28 | 0.12 | 0.34 | 0.23 |
| std. dev. | 0.25 | 0.11 | 0.25 | 0.23 |
| max. abs. | 0.71 | 0.47 | 1.10 | 0.56 |
| median abs. | 0.17 | 0.08 | 0.18 | 0.12 |

[a]The PBE0 functional was used in the TDDFT and ev*GW*-BSE calculations.

**Table 4. Deviations of Triplet Excitation Energies (eV) Obtained in the aug-cc-pVTZ Basis with Respect to the CC3/aug-cc-pVTZ Reference[a]**

| | TDDFT | CC2 | ev*GW*-BSE | qs*GW*-BSE |
|---|---|---|---|---|
| mean | −0.50 | 0.13 | −0.84 | −0.52 |
| mean abs. | 0.50 | 0.14 | 0.84 | 0.52 |
| RMS | 0.54 | 0.17 | 0.90 | 0.55 |
| std. dev. | 0.22 | 0.12 | 0.33 | 0.20 |
| max. abs. | 0.96 | 0.47 | 1.97 | 1.07 |
| median abs. | 0.49 | 0.11 | 0.84 | 0.52 |

[a]The PBE0 functional was used in the TDDFT and ev*GW*-BSE calculations.

**Table 5. Deviations of Singlet Excitation Energies (eV) Obtained in the aug-cc-pVTZ Basis with Respect to the def2-TZVP Results[a]**

| | TDDFT | CC2 | ev*GW*-BSE | qs*GW*-BSE |
|---|---|---|---|---|
| mean | −0.07 | −0.11 | −0.22 | −0.08 |
| mean abs. | 0.08 | 0.11 | 0.22 | 0.08 |
| RMS | 0.12 | 0.16 | 0.29 | 0.11 |
| std. dev. | 0.10 | 0.11 | 0.19 | 0.07 |
| max. abs. | 0.53 | 0.53 | 1.02 | 0.46 |
| median abs. | 0.04 | 0.08 | 0.15 | 0.06 |

[a]The PBE0 functional was used in the TDDFT and ev*GW*-BSE calculations.

**Table 6. Deviations of Triplet Excitation Energies (eV) Obtained in the aug-cc-pVTZ Basis with Respect to the def2-TZVP Results[a]**

| | TDDFT | CC2 | ev*GW*-BSE | qs*GW*-BSE |
|---|---|---|---|---|
| mean | −0.02 | −0.05 | −0.28 | −0.03 |
| mean abs. | 0.02 | 0.05 | 0.28 | 0.03 |
| RMS | 0.03 | 0.08 | 0.38 | 0.04 |
| std. dev. | 0.02 | 0.06 | 0.25 | 0.03 |
| max. abs. | 0.10 | 0.44 | 1.01 | 0.14 |
| median abs. | 0.02 | 0.03 | 0.21 | 0.03 |

[a]The PBE0 functional was used in the TDDFT and ev*GW*-BSE calculations.



DOI: 10.1021/acs.jctc.8b00014
J. Chem. Theory Comput. 2018, 14, 2127−2136

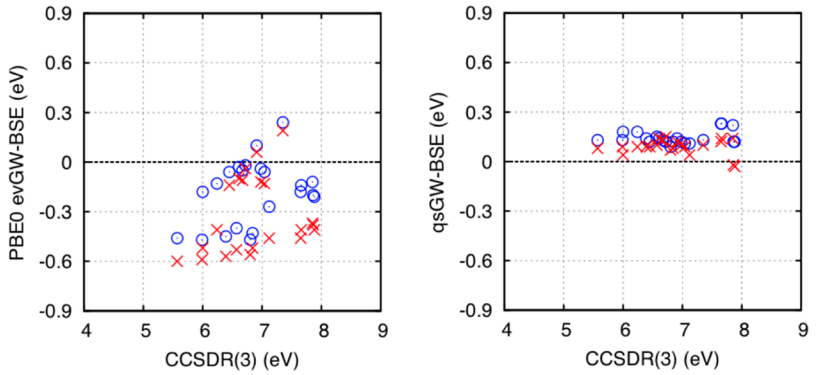


**Figure 4.** Rydberg excitation energies computed in the def2-TZVP (blue circles) and def2-TZVPD (red crosses) basis sets. Plotted are the deviations from the CCSDR(3) reference.

mutual comparisons between the def2-TZVP and aug-cc-pVTZ basis sets. For CC2, TDDFT, and qs*GW*-BSE, the extension of the basis set with diffuse functions only leads to slight lowering in the excitation energies, and the def2-TZVP and aug-cc-pVTZ results are in perfect agreement. The basis-set dependence is, however, much more pronounced for the ev*GW*-BSE model. Compared to the other three methods, the lowering in the ev*GW*-BSE excitation energies due to the diffuse functions is twice as large for singlet states and even an order of magnitude larger for triplet states. This remarkable overstabilization results in much less accurate excitation energies obtained from ev*GW*-BSE with the more diffuse basis set. For a closer look at this problem, we have computed the ev*GW*-BSE excitation energies with various basis sets for a selected subset of 10 molecules (see Supporting Information for details). Within a series of basis sets, that is, within the sets def2-XZVP, def2-XZVPD, or aug-cc-pVXZ, ev*GW*-BSE exhibits normal basis-set convergence behavior. However, when the basis sets are extended by diffuse functions, unusual energy lowering can be observed in some cases, especially for acetamide and propanamide, which leads to the deterioration in the excitation energies with respect to the reference values. The reason for the large basis-set dependence of ev*GW*-BSE is not clear yet, and further studies are required. At this stage, the medium-sized def2-TZVP basis set is recommended for the ev*GW*-BSE model, but it must be kept in mind that the good performance of ev*GW*-BSE at the def2-TZVP level is to some extent due to error cancellation.

**4.2. Rydberg States.** The benchmark set developed by Sauer and co-workers[47] consists of benzene and five polycyclic aromatic hydrocarbons with 39 valence and 76 Rydberg states. In the calculations, extra diffuse functions were added to the center of mass of the molecules for a proper treatment of the Rydberg states. We have computed the ev*GW*-BSE and qs*GW*-BSE excitation energies of 22 Rydberg states in benzene and naphthalene using the def2-TZVP and def2-TZVPD basis set plus the additional molecule-centered diffuse functions of ref 47 (see Supporting Information for details). The geometries and coupled-cluster reference values—here, the CCSDR(3) approximation was used, which is a noniterative analog to the CC3 model—are the same as in ref 47. The errors in the computed ev*GW*-BSE and qs*GW*-BSE excitation energies are plotted against the CCSDR(3) reference values in Figure 4, and the statistical analysis is listed in Table 7. The qs*GW*-BSE results exhibit small basis-set dependence and very good agreement with the CCSDR(3) reference values, whereas ev*GW*-BSE gives on average too low energies, and again, the excitation energies are overstabilized when using the more diffuse basis set.

**Table 7. Deviations of ev*GW*-BSE and qs*GW*-BSE Rydberg Excitation Energies (eV) Obtained in the def2-TZVP and def2-TZVPD Basis with Respect to the CCSDR(3) Reference**

| | ev*GW*-BSE | | qs*GW*-BSE | |
|---|---|---|---|---|
| | def2-TZVP | def2-TZVPD | def2-TZVP | def2-TZVPD |
| mean | −0.18 | −0.33 | 0.14 | 0.09 |
| mean abs. | 0.21 | 0.35 | 0.14 | 0.09 |
| RMS | 0.27 | 0.40 | 0.15 | 0.10 |
| std. dev. | 0.20 | 0.23 | 0.04 | 0.05 |
| max. abs. | 0.47 | 0.60 | 0.23 | 0.15 |
| median abs. | 0.18 | 0.41 | 0.13 | 0.09 |

**4.3. Charge-Transfer States.** We investigated the charge-transfer (CT) states of *para*-nitroaniline (*p*NA), dimethylaminobenzonitrile (DMABN), the benzene−tetracyanoethylene complex (B-TCNE), phenylpyrrole (PP), and HCl. The geometries were taken from ref 5 for *p*NA, DMABN ($C_{2v}$), and B-TCNE and from ref 48 for DMABN ($C_s$), PP, and HCl. The excitation energies were calculated at the ev*GW*-BSE/def2-TZVP and qs*GW*-BSE/def2-TZVP levels. The degree of CT was quantified using a diagnostic Λ similar to the one proposed by Tozer and co-workers.[48] In the present work, we compute this diagnostic from the spatial overlap between the dominating occupied and virtual NTOs of the respective excitation,

$$\Lambda = \int |\varphi_{\mathrm{occ}}^{\mathrm{NTO}}(\mathbf{r})\varphi_{\mathrm{vir}}^{\mathrm{NTO}}(\mathbf{r})|\, \mathrm{d}^3\mathbf{r} \tag{15}$$

Also in the case of the CT excitations, we adopt the corresponding CC3/aug-cc-pVTZ results as reference data, except for the benzene−tetracyanoethylene complex, where the CC3/aug-cc-pVTZ calculation was too time consuming. In the B-TCNE case, we compare with CC2/aug-cc-pVTZ results. The results are collected in Table 8. As shown in Figure 5, the ev*GW*-BSE/def2-TZVP and qs*GW*-BSE/def2-TZVP results are in good mutual agreement with each other and compare well with the reference values. In comparison with TDDFT, the BSE formalism has the important advantage that there are no obvious problems with the computation of CT states nor with the occurrence of spurious CT states that easily crop up at the TDDFT level.



DOI: 10.1021/acs.jctc.8b00014
J. Chem. Theory Comput. 2018, 14, 2127−2136

**Table 8. Singlet Excitation Energies (eV) and Diagnostics Λ of Charge-Transfer (CT) States**

| | | evGW-BSE | | qsGW-BSE | | |
|---|---|---|---|---|---|---|
| molecule | state | ΔE | Λ | ΔE | Λ | reference value |
| pNA | $2^1A_1$ | 4.47 | 0.61 | 4.42 | 0.63 | 4.39[a] |
| DMABN ($C_{2v}$) | $2^1A_1$ | 4.86 | 0.74 | 4.81 | 0.75 | 4.86[a] |
| DMABN ($C_s$) | $2^1A'$ | 4.80 | 0.75 | 4.75 | 0.75 | 4.75[a] |
| B-TCNE | $2^1A_1$ | 3.45 | 0.20 | 3.55 | 0.16 | 3.41[b] |
| PP | $2^1B_2$ | 5.18 | 0.63 | 5.23 | 0.62 | 5.21[a] |
| | $3^1A_1$ | 5.92 | 0.24 | 5.96 | 0.29 | 5.69[a] |
| HCl | $1^1\Pi$ | 7.66 | 0.51 | 8.07 | 0.49 | 7.81[c] |

[a]Estimated CC3/aug-cc-pVTZ results based on CC3/TZVP and CC2/aug-cc-pVTZ results. [b]CC2/aug-cc-pVTZ result. [c]CC3/aug-cc-pVTZ result.

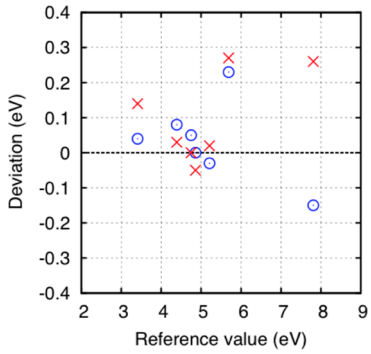


**Figure 5.** Computed evGW-BSE (blue circles) and qsGW-BSE (red crosses) excitation energies of CT states. Plotted are the deviations from the reference values.

## 5. PERFORMANCE ASSESSMENT

**5.1. Timings.** Tables 9 and 10 give the timings for the TDDFT, CC2, and GW-BSE computations of 40 singlet excitation energies (five in each irreducible representation of the $D_{2h}$ point group) of five aromatic hydrocarbons: benzene, naphthalene, anthracene, tetracene, and pentacene.

Table 9 shows that the CPU times for the TDDFT and BSE approaches are of the same order of magnitude, as expected.[27] Furthermore, the CPU times for the evGW part of the calculations are fully acceptable, which is quite remarkable concerning the fact that the full time-dependent Hartree (TDH) response function is determined in every iteration in order to compute quasiparticle energies for all orbital levels. The corresponding matrix is diagonalized very efficiently. The CPU times for the qsGW calculations are an order of magnitude larger than for the evGW case, partly because many more iterations were needed to converge the calculations. However, since in the present work we have observed only a minor advantage of the qsGW method over the evGW method, we recommend using the latter for real-world applications of the Bethe−Salpeter formalism.

The dRPA-response part of our GW code has been parallelized, but since not all parts of the whole calculation have been parallelized, the parallel efficiency is not very high on 8 or 16 processors (Table 10). According to Amdahl's law, the speedup is limited by the serial part of the code. Nevertheless, Table 10 shows that in particular evGW calculations on larger systems such as pentacene in the def2-TZVP basis can be performed in reasonable time (ca. 17 min) on a standard Intel Xeon server node. Compared to the initial $G_0W_0$ implementation in TURBOMOLE, the new code is approximately 20 (48) times faster for the benzene (naphthalene) molecule.

**5.2. $(C_{60})_2$.** In order to assess the performance of our improved implementation of the GW approximation in the TURBOMOLE program package, we have computed the ordinary photoabsorption (OPA) spectrum of the $(C_{60})_2$ system shown in Figure 6. This molecular system displays $D_{2h}$ symmetry. The computations were performed in the def2-TZVP basis comprising 3720 functions in total. The corresponding "MP2-fitting" auxiliary basis comprised 9120 functions. The total tensor spaces (number of occupied−virtual orbital products) for excitations to $B_{1u}$, $B_{2u}$, and $B_{3u}$ excited states amounted to 151 638, 151 198, and 151 210, respectively. The absorption spectrum, which is governed by excitations belonging to these three electric-dipole-allowed irreducible representations, is shown in Figure 7. The BSE calculations are based on the PBE0 functional and $G_0W_0$ quasiparticle energies. Fifteen excitations were computed in each irreducible representation. The BSE calculation took ca. three days on eight cores of an Intel Xeon E5-2687W v4 @ 3.00 GHz processor, while the underlying $G_0W_0$ calculation took ca. 18 days on 12 cores on the same processor.

**5.3. $C_{84}$ Fullerene.** In order to assess the performance of our improved implementation of the GW approximation in the TURBOMOLE program package further, we have also studied a $D_2$-symmetric isomer of the fullerene $C_{84}$. As this is a chiral isomer, it offers the opportunity to simulate an electronic circular-dichroism (ECD) spectrum based on BSE calculations of singlet excited states.

The calculations were performed for the enantiomer with ($^fA$) configuration according to the configurational descriptor system of Thilgen, Herrmann, and Diederich (Figure 8).[49] Experimental ECD spectra were already reported for this enantiomer in the literature in the 1990s.[50,51] TDDFT investigations followed soon.[52−54]

In the present work, we have optimized the equilibrium structure of the ($^fA$)-$D_2$-$C_{84}$ enantiomer at the PBE0/def2-SVP

**Table 9. CPU Times (min) for TDDFT, CC2,and GW-BSE Computations in the def2-TZVP Basis on a Single Core of an Intel Xeon E5-2687W v2 (25M Cache, 3.40 GHz) Processor[a]**

| | | | evGW-BSE | | qsGW-BSE | |
|---|---|---|---|---|---|---|
| | TDDFT | CC2 | evGW | BSE | qsGW | BSE |
| benzene | 1.4(8) | 3.8 | 0.4(6) | 0.7(11) | 2.5(13) | 0.7(11) |
| naphthalene | 5.1(9) | 19.6 | 2.3(5) | 3.3(15) | 23.7(17) | 3.2(13) |
| anthracene | 12.5(8) | 62.1 | 9.4(5) | 9.4(13) | 122.7(21) | 9.6(13) |
| tetracene | 24.9(11) | 142.6 | 35.6(6) | 20.4(15) | 510.9(28) | 20.8(15) |
| pentacene | 44.8(9) | 309.5 | 88.8(4) | 41.5(18) | 851.4(16) | 40.4(16) |

[a]The number of iterations is given in the parentheses.



DOI: 10.1021/acs.jctc.8b00014
J. Chem. Theory Comput. 2018, 14, 2127−2136

Table 10. Wall Clock Times (min) for *GW* Computations in the def2-TZVP Basis on Different Numbers of Cores of an Intel Xeon E5-2687W v2 (25M Cache, 3.40 GHz) Processor

| | ev*GW* | | | | | qs*GW* | | | | |
|---|---|---|---|---|---|---|---|---|---|---|
| | 1[a] | 2[a] | 4[a] | 8[a] | 16[a] | 1[a] | 2[a] | 4[a] | 8[a] | 16[a] |
| benzene | 0.4 | 0.4 | 0.4 | 0.4 | 0.4 | 2.5 | 2.2 | 1.7 | 1.4 | 1.2 |
| naphthalene | 2.3 | 1.8 | 1.6 | 1.6 | 1.6 | 23.7 | 20.3 | 12.8 | 9.1 | 8.0 |
| anthracene | 9.4 | 6.5 | 5.2 | 4.4 | 4.2 | 122.8 | 107.0 | 63.9 | 41.1 | 31.0 |
| tetracene | 35.6 | 23.0 | 15.9 | 12.4 | 11.4 | 511.3 | 436.5 | 246.2 | 149.7 | 105.2 |
| pentacene | 88.9 | 56.1 | 33.5 | 22.0 | 16.7 | 852.1 | 707.2 | 383.4 | 216.7 | 135.9 |

[a]Number of cores.

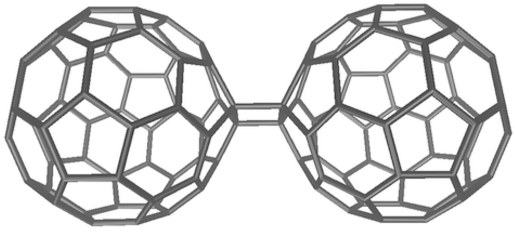

Figure 6. PBE0/def2-TZVP structure of $(C_{60})_2$.

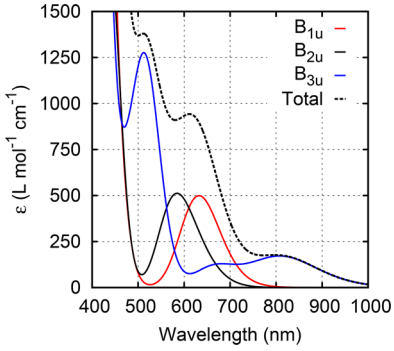


Figure 7. Ordinary photoabsorption spectrum of $(C_{60})_2$. In the simulation, the bands were broadened by means of Gaussians with full width at half-maximum (fwhm) of 2500 cm$^{-1}$.

Figure 8. PBE0/def2-SVP structure of $(^fA)$-$D_2$-$C_{84}$.

level, we have determined the quasiparticle energies at the ev*GW* level, and we have computed 150 excitation energies (50 excitations in each of the irreducible representations $B_1$, $B_2$, and $B_3$) and rotatory strengths using the BSE formalism. From these energies and rotatory strengths, we have simulated the ECD spectrum shown in Figure 9. In the simulation, the bands were broadened by means of Gaussians with full width at half-maximum (fwhm) of 0.35 eV, and the computed rotatory strengths were scaled by a factor of 1/14. This is the same puzzling scaling factor as used in ref 52, and the discrepancy between theory and experiment has still not been resolved. We would like to stress at this point that the simulated spectrum was neither red- nor blue-shifted.

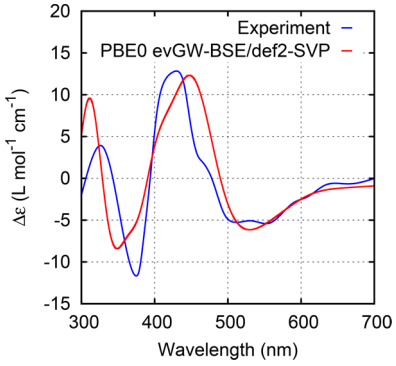


Figure 9. Simulated ECD spectrum of $(^fA)$-$D_2$-$C_{84}$ compared to experiment (ref 50). Gaussian broadening with fwhm = 0.35 eV. Calculated rotatory strengths were scaled with the factor 1/14.

For $C_{84}$, the def2-SVP basis comprises 1176 basis functions. With 252 doubly occupied orbitals, this yields a total tensor space of dimension 232,848. Fortunately, exploiting $D_2$ symmetry reduces the complexity of the calculation to four tensor spaces of sizes 58 206, 58 210, 58 216, and 58 216 for the four irreducible representations of the point group. On eight cores of an Intel Xeon E5-2687W v4 @ 3.00 GHz processor, the ev*GW* calculation took 65 h (five iterations). The subsequent BSE calculation took 185 h on a single core of an Intel Xeon E5-4640 @ 2.40 GHz processor.

## 6. CONCLUSIONS

The aim of the present article is to demonstrate that the Bethe−Salpeter formalism is an interesting and valid alternative to the time-dependent DFT approach and that the CPU and wall-clock computation times of both the Bethe−Salpeter calculations themselves as well as the underlying *GW* calculations of the required quasiparticle energies are fully acceptable, thus allowing for real-world applications of the theory. It is remarkable that this is even true when computing the quasiparticle energies for *all* orbital levels, which in the present work is achieved by means of evaluating the full spectral function in a molecular-orbital formalism.

## ■ ASSOCIATED CONTENT

### Supporting Information

The Supporting Information is available free of charge on the ACS Publications website at DOI: 10.1021/acs.jctc.8b00014.

Tables with excitation energies of singlet and triplet valence states, Rydberg states, and charge-transfer states; values obtained in various basis sets are given for a selected set of molecules; occupied-virtual pairs of natural transition orbitals obtained from qs*GW*-BSE



DOI: 10.1021/acs.jctc.8b00014
J. Chem. Theory Comput. 2018, 14, 2127−2136

calculations on the charge-transfer states are depicted (PDF)

## AUTHOR INFORMATION


### Corresponding Author

*(W.K.) E-mail: klopper@kit.edu. Fax: +49 721 60847225.

### ORCID

Wim Klopper: 0000-0002-5219-9328



### Funding

C.H. gratefully acknowledges financial support by the Deutsche Forschungsgemeinschaft (DFG) through the Priority Programme 1807 (Control of London Dispersion Interactions in Molecular Chemistry). X.G. gratefully acknowledges financial support by the DFG through the Transregional Collaborative Research Centre 88 [Cooperative Effects in Homo- and Heterometallic Complexes (3MET)].


### Notes

The authors declare no competing financial interest.

## REFERENCES


(1) Ziaei, V.; Bredow, T. Simple many-body based screening mixing ansatz for improvement of *GW*/Bethe-Salpeter equation excitation energies of molecular systems. *Phys. Rev. B: Condens. Matter Mater. Phys.* **2017**, *96*, 195115.

(2) Rangel, T.; Hamed, S. M.; Bruneval, F.; Neaton, J. B. An assessment of low-lying excitation energies and triplet instabilities of organic molecules with an ab initio Bethe-Salpeter equation approach and the Tamm-Dancoff approximation. *J. Chem. Phys.* **2017**, *146*, 194108.

(3) Hung, L.; Bruneval, F.; Baishya, K.; Öğüt, S. Benchmarking the *GW* Approximation and Bethe-Salpeter Equation for Groups IB and IIB Atoms and Monoxides. *J. Chem. Theory Comput.* **2017**, *13*, 2135−2146.

(4) Azarias, C.; Habert, C.; Budzák, v.; Blase, X.; Duchemin, I.; Jacquemin, D. Calculations of *n*-$\pi$* Transition Energies: Comparisons Between TD-DFT, ADC, CC, CASPT2, and BSE/*GW* Descriptions. *J. Phys. Chem. A* **2017**, *121*, 6122−6134.

(5) Jacquemin, D.; Duchemin, I.; Blase, X. Is the Bethe-Salpeter Formalism Accurate for Excitation Energies? Comparisons with TD-DFT, CASPT2, and EOM-CCSD. *J. Phys. Chem. Lett.* **2017**, *8*, 1524−1529.

(6) Escudero, D.; Duchemin, I.; Blase, X.; Jacquemin, D. Modeling the Photochrome-$TiO_2$ Interface with Bethe-Salpeter and Time-Dependent Density Functional Theory Methods. *J. Phys. Chem. Lett.* **2017**, *8*, 936−940.

(7) Jacquemin, D.; Duchemin, I.; Blondel, A.; Blase, X. Benchmark of Bethe-Salpeter for Triplet Excited-States. *J. Chem. Theory Comput.* **2017**, *13*, 767−783.

(8) Azarias, C.; Duchemin, I.; Blase, X.; Jacquemin, D. Bethe-Salpeter study of cationic dyes: Comparisons with ADC(2) and TD-DFT. *J. Chem. Phys.* **2017**, *146*, 034301.

(9) Ziaei, V.; Bredow, T. *GW*-BSE approach on $S_1$ vertical transition energy of large charge transfer compounds: A performance assessment. *J. Chem. Phys.* **2016**, *145*, 174305.

(10) Bruneval, F.; Rangel, T.; Hamed, S. M.; Shao, M.; Yang, C.; Neaton, J. B. molgw 1: Many-body perturbation theory software for atoms, molecules, and clusters. *Comput. Phys. Commun.* **2016**, *208*, 149−161.

(11) Cardia, R.; Malloci, G.; Rignanese, G.-M.; Blase, X.; Molteni, E.; Cappellini, G. Electronic and optical properties of hexathiapentacene in the gas and crystal phases. *Phys. Rev. B: Condens. Matter Mater. Phys.* **2016**, *93*, 235132.

(12) Blase, X.; Boulanger, P.; Bruneval, F.; Fernandez-Serra, M.; Duchemin, I. *GW* and Bethe-Salpeter study of small water clusters. *J. Chem. Phys.* **2016**, *144*, 034109.

(13) Jacquemin, D.; Duchemin, I.; Blondel, A.; Blase, X. Assessment of the Accuracy of the Bethe-Salpeter (BSE/*GW*) Oscillator Strengths. *J. Chem. Theory Comput.* **2016**, *12*, 3969−3981.

(14) Duchemin, I.; Jacquemin, D.; Blase, X. Combining the *GW* formalism with the polarizable continuum model: A state-specific non-equilibrium approach. *J. Chem. Phys.* **2016**, *144*, 164106.

(15) Jacquemin, D.; Duchemin, I.; Blase, X. Assessment of the convergence of partially self-consistent BSE/*GW* calculations. *Mol. Phys.* **2016**, *114*, 957−967.

(16) Jacquemin, D.; Duchemin, I.; Blase, X. 0−0 Energies Using Hybrid Schemes: Benchmarks of TD-DFT, CIS(D), ADC(2), CC2, and BSE/GW formalisms for 80 Real-Life Compounds. *J. Chem. Theory Comput.* **2015**, *11*, 5340−5359.

(17) Jacquemin, D.; Duchemin, I.; Blase, X. Benchmarking the Bethe-Salpeter Formalism on a Standard Organic Molecular Set. *J. Chem. Theory Comput.* **2015**, *11*, 3290−3304.

(18) Baumeier, B.; Rohlfing, M.; Andrienko, D. Electronic Excitations in Push-Pull Oligomers and Their Complexes with Fullerene from Many-Body Green's Functions Theory with Polarizable Embedding. *J. Chem. Theory Comput.* **2014**, *10*, 3104−3110.

(19) Boulanger, P.; Chibani, S.; Le Guennic, B.; Duchemin, I.; Blase, X.; Jacquemin, D. Combining the Bethe-Salpeter Formalism with Time-Dependent DFT Excited-State Forces to Describe Optical Signatures: NBO Fluoroborates as Working Examples. *J. Chem. Theory Comput.* **2014**, *10*, 4548−4556.

(20) Boulanger, P.; Jacquemin, D.; Duchemin, I.; Blase, X. Fast and Accurate Electronic Excitations in Cyanines with the Many-Body Bethe-Salpeter Approach. *J. Chem. Theory Comput.* **2014**, *10*, 1212−1218.

(21) Duchemin, I.; Blase, X. Resonant hot charge-transfer excitations in fullerene-porphyrin complexes: Many-body Bethe-Salpeter study. *Phys. Rev. B: Condens. Matter Mater. Phys.* **2013**, *87*, 245412.

(22) Faber, C.; Boulanger, P.; Duchemin, I.; Attaccalite, C.; Blase, X. Many-body Green's function *GW* and Bethe-Salpeter study of the optical excitations in a paradigmatic model dipeptide. *J. Chem. Phys.* **2013**, *139*, 194308.

(23) Baumeier, B.; Andrienko, D.; Rohlfing, M. Frenkel and Charge-Transfer Excitations in Donor-acceptor Complexes from Many-Body Green's Functions Theory. *J. Chem. Theory Comput.* **2012**, *8*, 2790−2795.

(24) Faber, C.; Duchemin, I.; Deutsch, T.; Blase, X. Many-body Green's function study of coumarins for dye-sensitized solar cells. *Phys. Rev. B: Condens. Matter Mater. Phys.* **2012**, *86*, 155315.

(25) Duchemin, I.; Deutsch, T.; Blase, X. Short-Range to Long-Range Charge-Transfer Excitations in the Zincbacteriochlorin-Bacteriochlorin Complex: A Bethe-Salpeter Study. *Phys. Rev. Lett.* **2012**, *109*, 167801.

(26) Blase, X.; Attaccalite, C. Charge-transfer excitations in molecular donor-acceptor complexes within the many-body Bethe-Salpeter approach. *Appl. Phys. Lett.* **2011**, *99*, 171909.

(27) Krause, K.; Klopper, W. Implementation of the Bethe- Salpeter equation in the TURBOMOLE program. *J. Comput. Chem.* **2017**, *38*, 383−388.

(28) Furche, F.; Ahlrichs, R.; Hättig, C.; Klopper, W.; Sierka, M.; Weigend, F. Turbomole. *WIREs: Comput. Mol. Sci.* **2014**, *4*, 91−100.

(29) *TURBOMOLE*, V7.2 2017; a development of University of Karlsruhe and Forschungszentrum Karlsruhe GmbH, 1989−2007; TURBOMOLE GmbH: since 2007; available from http://www.turbomole.com.

(30) Blase, X.; Attaccalite, C.; Olevano, V. First-principles *GW* calculations for fullerenes, porphyrins, phtalocyanine, and other molecules of interest for organic photovoltaic applications. *Phys. Rev. B: Condens. Matter Mater. Phys.* **2011**, *83*, 115103.

(31) Govoni, M.; Galli, G. Large Scale GW Calculations. *J. Chem. Theory Comput.* **2015**, *11*, 2680−2696.

(32) Wilhelm, J.; Del Ben, M.; Hutter, J. *GW* in the Gaussian and plane waves scheme with application to linear acenes. *J. Chem. Theory Comput.* **2016**, *12*, 3623−3635.




DOI: 10.1021/acs.jctc.8b00014
*J. Chem. Theory Comput.* 2018, 14, 2127−2136

(33) Vlček, V.; Rabani, E.; Neuhauser, D.; Baer, R. Stochastic *GW* Calculations for Molecules. *J. Chem. Theory Comput.* **2017**, *13*, 4997−5003.
(34) van Setten, M. J.; Weigend, F.; Evers, F. The *GW*-method for Quantum Chemistry Applications: Theory and Implementation. *J. Chem. Theory Comput.* **2013**, *9*, 232−246.
(35) Krause, K.; Harding, M. E.; Klopper, W. Coupled-cluster reference values for the GW27 and GW100 test sets for the assessment of *GW* methods. *Mol. Phys.* **2015**, *113*, 1952−1960.
(36) Koval, P.; Foerster, D.; Sánchez-Portal, D. Fully self-consistent *GW* and quasiparticle self-consistent *GW* for molecules. *Phys. Rev. B: Condens. Matter Mater. Phys.* **2014**, *89*, 155417.
(37) Caruso, F.; Rinke, P.; Ren, X.; Rubio, A.; Scheffler, M. Self-consistent *GW*: All-electron implementation with localized basis functions. *Phys. Rev. B: Condens. Matter Mater. Phys.* **2013**, *88*, 075105.
(38) Caruso, F.; Rinke, P.; Ren, X.; Scheffler, M.; Rubio, A. Unified description of ground and excited states of finite systems: The self-consistent *GW* approach. *Phys. Rev. B: Condens. Matter Mater. Phys.* **2012**, *86*, 081102.
(39) van Schilfgaarde, M.; Kotani, T.; Faleev, S. Quasiparticle Self-Consistent *GW* Theory. *Phys. Rev. Lett.* **2006**, *96*, 226402.
(40) Kaplan, F.; Harding, M. E.; Seiler, C.; Weigend, F.; Evers, F.; van Setten, M. J. Quasi-Particle Self-Consistent *GW* for Molecules. *J. Chem. Theory Comput.* **2016**, *12*, 2528−2541.
(41) Bauernschmitt, R.; Ahlrichs, R. Treatment of electronic excitations within the adiabatic approximation of time dependent density functional theory. *Chem. Phys. Lett.* **1996**, *256*, 454−464.
(42) Schreiber, M.; Silva-Junior, M. R.; Sauer, S. P. A.; Thiel, W. Benchmarks for electronically excited states: CASPT2, CC2, CCSD, and CC3. *J. Chem. Phys.* **2008**, *128*, 134110.
(43) Silva-Junior, M. R.; Sauer, S. P. A.; Schreiber, M.; Thiel, W. Basis set effects on coupled cluster benchmarks of electronically excited states: CC3, CCSDR(3) and CC2. *Mol. Phys.* **2010**, *108*, 453−465.
(44) Silva-Junior, M. R.; Schreiber, M.; Sauer, S. P. A.; Thiel, W. Benchmarks of electronically excited states: Basis set effects on CASPT2 results. *J. Chem. Phys.* **2010**, *133*, 174318.
(45) Kánnár, D.; Szalay, P. G. Benchmarking Coupled Cluster Methods on Valence Singlet Excited States. *J. Chem. Theory Comput.* **2014**, *10*, 3757−3765.
(46) Kánnár, D.; Szalay, P. G. Benchmarking coupled cluster methods on singlet excited states of nucleobases. *J. Mol. Model.* **2014**, *20*, 2503.
(47) Falden, H. H.; Falster-Hansen, K. R.; Bak, K. L.; Rettrup, S.; Sauer, S. P. A. Benchmarking Second Order Methods for the Calculation of Vertical Electronic Excitation Energies: Valence and Rydberg States in Polycyclic Aromatic Hydrocarbons. *J. Phys. Chem. A* **2009**, *113*, 11995.
(48) Peach, M. J. G.; Benfield, P.; Helgaker, T.; Tozer, D. J. Excitation energies in density functional theory: An evaluation and a diagnostic test. *J. Chem. Phys.* **2008**, *128*, 044118.
(49) Thilgen, C.; Herrmann, A.; Diederich, F. Configurational Description of Chiral Fullerenes and Fullerene Derivatives with a Chiral Functionalization Pattern. *Helv. Chim. Acta* **1997**, *80*, 183−199.
(50) Hawkins, J. M.; Nambu, M.; Meyer, A. Resolution and Configurational Stability of the Chiral Fullerenes C76, C78, and C84: A Limit for the Activation Energy of the Stone-Wales Transformation. *J. Am. Chem. Soc.* **1994**, *116*, 7642−7645.
(51) Crassous, J.; Rivera, J.; Fender, N. S.; Shu, L.; Echegoyen, L.; Thilgen, C.; Herrmann, A.; Diederich, F. Chemistry of $C_{84}$: Separation of Three Constitutional Isomers and Optical Resolution of $D_2$-$C_{84}$ by Using the "Bingel-Retro-Bingel" Strategy. *Angew. Chem., Int. Ed.* **1999**, *38*, 1613−1617.
(52) Furche, F.; Ahlrichs, R. Absolute Configuration of $D_2$-Symmetric Fullerene $C_{84}$. *J. Am. Chem. Soc.* **2002**, *124*, 3804−3805.
(53) Jiemchooroj, A.; Norman, P. Electronic circular dichroism spectra from the complex polarization propagator. *J. Chem. Phys.* **2007**, *126*, 134102.
(54) Hidalgo, F.; Noguez, C. Optically active nanoparticles: Fullerenes, carbon nanotubes, and metal nanoparticles. *Phys. Status Solidi B* **2010**, *247*, 1889−1897.


DOI: 10.1021/acs.jctc.8b00014
*J. Chem. Theory Comput.* 2018, 14, 2127−2136